Kinematic Analysis and Design of Suspension-steering Mechanisms for Vehicles

Prof. Nobuyuki IWATSUKI

Dr. Eng, Tokyo Institute of Technology

Aiming to understand suspension and steering mechanisms for vehicles, kinematic analysis of the MacPherson strut suspension mechanism and Ackermann-Jeantaud scheme steering mechanism which are frequently used in front engine-front drive small cars is explained based on the essential spatial geometry and vector analysis. Motion performance of vehicles due to the mechanisms is quantitatively evaluated with the fluctuation of turning center and the transmissibility of steering mechanism. The process and results of the optimum design of the mechanisms based on the criteria of the motion performance are then explained.

Key Words: steering mechanism, suspension mechanism, spatial linkage, kinematics, mechanism design, optimization

1. Introduction

Vehicle wheels are supported by a suspension mechanism to absorb the vibrations caused by unevenness in the travel surface. A steering mechanism rotates front wheels around the vertical axis to turn the vehicle. Especially in FF (front-engine, front-wheel drive) vehicles, a complex spatial link mechanism where a wheel driving mechanism is incorporated in the suspension and steering mechanisms is packed in confined space and can be viewed as an art work of mechanical device. The suspension and steering mechanisms have also progressed over the long history of vehicles, and can be considered to be almost technically completed. But higher-performance electric power steering devices and the rise of electric vehicles have recently been creating the potential for vehicle drive system innovations and new four-wheel independent steering methods. New designs of the suspension and steering mechanisms will then be required.

New designs call for learning from the past by analyzing past mechanisms to thoroughly understand their designs. But ever-advancing vehicle design information is a corporate trade secret not accessible in detail. The author is a university professor specializing in link mechanisms and machine elements, and with previously little interest or knowledge in vehicle mechanisms. But when examining suspension and steering mechanisms, the author found that many vehicle guidebooks and manuals[1]-[5] showed many diagrams and photos without dimensions and specifications and did not explain

the quantitative evaluations of suspension or steering performance in detail. On a more practical level, there was not enough information that could be included in teaching materials used to teach or instruct students in courses such as mechanical kinematics.

In this article, the kinematic analysis and the quantitative evaluation of motion performance of the suspension and steering mechanisms which are frequently used in commercial vehicles are explained based on the kinematics of the spatial linkage and the optimum design to improve the motion performance is then tried.

As mentioned, suspension and steering mechanisms have a long history of research and development. Therefore, each car builder accumulates expertise individually. The kinematic analysis presented in this article is just a kinematic analysis of a spatial linkage with rigid links. It is based on spatial geometry and vector analysis, and is not completely new method. However, since the black-box kinematic analysis with commercial software is recently becoming mainstream, it must be important to provide a geometry-based explanation conveying the essence of kinematic analysis. The author hopes that this article gives readers the better understanding of spatial linkage to apply to development of new mechanisms in future.

2. Suspension and Steering Mechanisms

2. 1 Suspension and Steering Mechanism Types

Axle suspension and independent suspension are the two main types of vehicle wheel suspension systems. Most passenger cars use independent suspension[1]–[6]. The various types of independent suspensions available include trailing-arm, MacPherson strut, double wishbone and multi-link types. Compact passenger cars commonly use MacPherson strut suspensions since they have few parts and enable compact designs. Steering systems commonly transmit steering wheel rotation via a steering shaft, convert it into the left-right linear motion of a rack bar, and rotate the left/right front wheels around the vertical axis via tie rods. The linear motion of the rack bar is obtained with a pinion-rack mechanism or a ball screw. Most of today's passenger cars use power assisted steering systems. Electric power steering systems use an assist motor to rotate the pinion or ball screw nut[1]–[6].

2. 2 Suspension and Steering Mechanisms to be Analyzed

This article deals with the MacPherson strut suspension mechanism commonly used in FF compact vehicles, along with the steering mechanism that converts the linear motion of the rack bar to rotate the front wheels via the tie rods. The motion conversion mechanism used to convert the rotation of the steering shaft to the linear motion of the rack bar is not discussed.

Figure 1 shows an overview of the mechanisms to be analyzed. Only the right-front wheel of an FF vehicle is shown in the figure. The hub carrier contains the wheel bearing that supports the drive shaft. It is supported by a strut composed of a spring and shock absorber, and by a suspension arm extending from the vehicle body. Steering is done by the linear displacement of the rack bar rotating the hub carrier around the kingpin axis via the tie rod and knuckle arm. The middle shaft keeps the wheel rotation speed constant during steering via two constant velocity joints.

Figure 2 shows **Fig. 1** represented as a mechanism diagram. The diagram shows only the right half of the suspension and steering mechanisms, ignoring the wheel drive system (the mechanism from the middle shaft to the wheel bearing). The suspension and steering mechanisms can be assumed as a spatial link mechanism. The degrees-of-freedom of the spatial link mechanism can be calculated using Grübler's formula as

$$F = 6(N-1) - \sum_{f=1}^{5}(6-f)J_f, \qquad (1)$$

where F is the mechanisms' degree-of-freedom, N is the number of links (including fixed links), f is the degree of freedom of a kinematic pair, and J_f is the number of
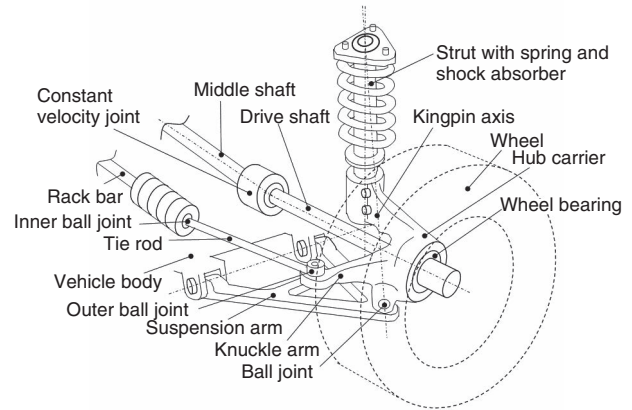
Fig. 1 Suspension and steering mechanisms to be analyzed
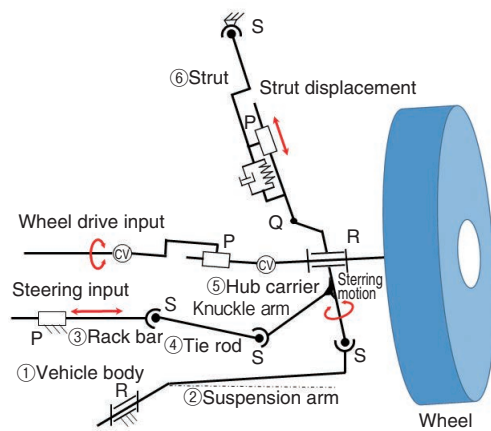
Fig. 2 Mechanism diagram of suspension and steering mechanisms

kinematic pairs having degree of freedom f. **Figure 2** shows that there are two prismatic pairs (P) and a revolute pair (R) with $f = 1$, and four spherical pairs (S) with $f=3$, therefore $J_1 = 3$, $J_3 = 4$ and $N=6$. Substituting these values into Eq. (1) yields:

$$F = 6(6-1) - [(6-1)3 + (6-3)4] = 3, \qquad (2)$$

indicating that the mechanisms are spatial link mechanisms with three degrees of freedom. Two of the inputs are the linear displacement of the rack bar, and the angular displacement of the suspension arm or the linear displacement of the strut. The other one degree of freedom is the rotation of the tie rod around the axis connecting the spherical pairs (ball joints) at both ends of the tie rod, which does not affect the motion of the suspension or steering. So this suspension-steering mechanism is a spatial link mechanism with two degrees-of-freedom, in which the input displacement of the suspension and the steering input are given independently.

3. Kinematic Analysis of Suspension and Steering Mechanisms

3. 1 Previous Research

Kinematic analysis of MacPherson strut suspension-steering mechanism has a long history with a highly extensive literature[7)–12)]. The research initially used a simplified model with coinciding strut and kingpin axes. This model later gave way to a detailed three-dimensional model, providing precise analysis. Analysis work often derives and solves closed-circuit vector equations of spatial mechanisms, and is difficult to understand geometrically. Researchers are also recently starting to analyze commercial multibody systems and solving for both motion and dynamics. However, such analysis is becoming a black box process.

This article therefore endeavors to explain the analysis procedure in a way that makes the geometry easy to understand.

3. 2 Analysis Procedure

Figure 3 is a mechanism diagram showing only the strut, hub carrier and tie rod of **Fig. 2**. A static coordinate system O-xyz is fixed to the vehicle body, and a moving coordinate system R$_{WC}$-$\xi\eta\zeta$ is set with the center of the front wheel as its origin and the axle as the $\hat{\xi}$ axis. Kinematic pairs are distinguished by two subscript letters that define each pair's position vector. For example, the spherical pair that connects the tie rod and knuckle arm on the hub carrier is written S$_{OB}$. Its position vector in the static coordinate system is written P_{OB}. The values given as mechanism constants are the tie rod length L_T, the R$_{WC}$-$\xi\eta\zeta$ coordinate system position vectors $\boldsymbol{p}_{SU}$, $\boldsymbol{p}_{OB}$ and $\boldsymbol{p}_{KP}$ of the spherical pair S$_{SU}$ at the strut top end, spherical pair S$_{OB}$ and kingpin spherical pair S$_{KP}$, as well as the unit direction vector $\boldsymbol{u}_S$ from the strut bottom end Q to strut top end S$_{SU}$.

As described in **Section 2**, the mechanism to be analyzed has two independent inputs. If these two inputs are assumed as a linear displacement of the rack bar and an angular displacement of the suspension arm, the position vector, P_{IB}, of spherical pair S$_{IB}$ connecting the rack bar and tie rod, and the position vector, P_{KP}, of the kingpin spherical pair S$_{KP}$ can be easily calculated.

The first step is to determine the strut displacement. The position vector of spherical pair S$_{SU}$ at the strut top end is given by the equation below in the R$_{WC}$-$\xi\eta\zeta$ coordinate system.

$$\boldsymbol{p}_{SU} = k\boldsymbol{u}_S + \boldsymbol{p}_{SB} \tag{3}$$
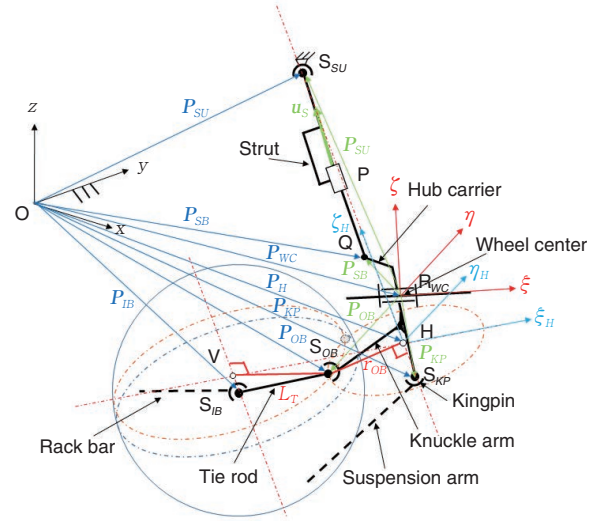
Fig. 3 Positions of kinematic pairs in the suspension and steering mechanisms

Expressing the distance between S$_{SU}$ and S$_{KP}$ in the O-xyz and R$_{WC}$-$\xi\eta\zeta$ coordinate systems yields $|\boldsymbol{p}_{SU} - \boldsymbol{p}_{KP}| = |P_{SU} - P_{KP}|$. Substituting Eq. (3) into this equation and solving the quadratic equation for k yields:

$$k = -\boldsymbol{u}_S \cdot (\boldsymbol{p}_{SB} - \boldsymbol{p}_{KP}) +$$
$$\sqrt{[\boldsymbol{u}_S \cdot (\boldsymbol{p}_{SB} - \boldsymbol{p}_{KP})]^2 - (\boldsymbol{p}_{SB} - \boldsymbol{p}_{KP}) \cdot (\boldsymbol{p}_{SB} - \boldsymbol{p}_{KP}) + (P_{SU} - P_{KP}) \cdot (P_{SU} - P_{KP})}. \tag{4}$$

The kingpin axis-direction unit direction vectors in the R$_{WC}$-$\xi\eta\zeta$ and O-xyz coordinate systems are given by the following equations.

$$\boldsymbol{u}_K = \frac{\boldsymbol{p}_{SU} - \boldsymbol{p}_{KP}}{|\boldsymbol{p}_{SU} - \boldsymbol{p}_{KP}|}, \quad U_K = \frac{P_{SU} - P_{KP}}{|P_{SU} - P_{KP}|} \tag{5}$$

The hub carrier acquires the S$_{OB}$ displacement and rotates around the kingpin axis. With H as the foot of the perpendicular descending from S$_{OB}$ to the kingpin axis, the position vector in the R$_{WC}$-$\xi\eta\zeta$ coordinate system is given as

$$\boldsymbol{p}_H = \ell\,\boldsymbol{u}_K + \boldsymbol{p}_{KP}. \tag{6}$$

The condition of orthogonality yields:

$$(\boldsymbol{p}_H - \boldsymbol{p}_{OB}) \cdot \boldsymbol{u}_K = 0. \tag{7}$$

Substituting Eq. (6) into Eq. (7) and solving for ℓ yields:

$$\ell = (\boldsymbol{p}_{OB} - \boldsymbol{p}_{KP}) \cdot \boldsymbol{u}_K. \tag{8}$$

The position vector of H in the O-xyz coordinate system is given by:

$$P_H = \ell\,U_H + P_{KP}, \tag{9}$$

and the distance between S$_{OB}$ and H is given by:

$$r_{OB} = \sqrt{(\boldsymbol{p}_{OB} - \boldsymbol{p}_H) \cdot (\boldsymbol{p}_{OB} - \boldsymbol{p}_H)}. \tag{10}$$

Viewing rotation around the kingpin axis as rotation by a revolute pair at H, the two links of $S_{IB} - S_{OB} - H$ are the two linkages of spherical pair – spherical pair – revolute pair. If the positions and postures of the revolute pair and spherical pairs at both ends are provided for these two linkages, the position of a spherical pair in between can be calculated[13]. In other words, the spherical pair S_{OB} is geometrically defined as the intersection of the sphere centered at S_{IB} with radius L_T (the tie rod length) and the circular ring with radius r_{OB} centered at H (**Fig. 3**).

To find this point of intersection, consider a spatial plane containing the circular ring with radius r_{OB} centered at H. A new moving coordinate system H-ξ_H η_H ζ_H with H as its origin is set in this plane. The ζ_H axis is set in the u_K direction. Let the ξ_H axis direction be the common normal to the ζ_H axis and a line that passes through S_{IB} and runs parallel to the ζ_H axis. Now we find point V, the other foot of this common normal. If the position vector of V in the O-xyz coordinate system is given by:

$$P_V = m U_K + P_{IB}. \tag{11}$$

The condition of orthogonality yields:

$$(P_H - P_V) \cdot U_K = 0. \tag{12}$$

So substituting Eq. (11) into Eq. (12) yields:

$$m = (P_H - P_{IB}) \cdot U_K. \tag{13}$$

From the position vectors obtained above, the unit direction vectors in the ζ_H, ξ_H and η_H axis directions can be written in the O-xyz coordinate system as:

$$K_H = U_H, \ \ I_H = \frac{P_H - P_V}{|P_H - P_V|}, \ \ J_H = K_H \times I_H. \tag{14}$$

Using the unit direction vectors of Eqs. (14), the coordinate transformation matrix for rotating from the H-ξ_H η_H ζ_H coordinate system to the O-xyz coordinate system is given by the formula below.

$$[T_H]^T = [I_H \quad J_H \quad K_H] \tag{15}$$

Figure 4 shows V, S_{OB} and H in the ξ_H η_H plane in the moving coordinate system H-ξ_H η_H ζ_H.

The position vector of S_{OB} in the H-ξ_H η_H ζ_H
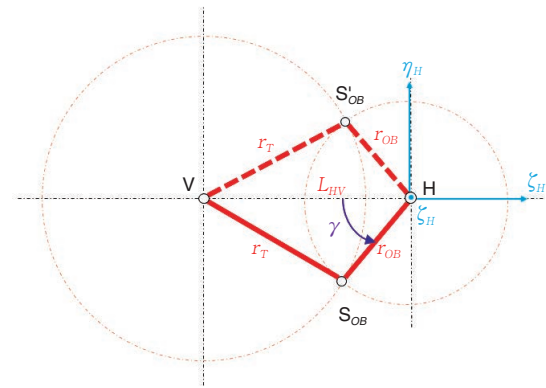
Fig. 4 Position of outer ball joint

coordinate system is therefore given geometrically by:

$$p_{OB,H} = \begin{bmatrix} r_{OB} \cos(\gamma - \pi) \\ r_{OB} \sin(\gamma - \pi) \\ 0 \end{bmatrix}, \tag{16}$$

where,

$$\gamma = \cos^{-1} \frac{r_{OB}^2 + L_{VH}^2 - r_T^2}{2 r_{OB} L_{VH}},$$
$$r_T = \sqrt{L_T^2 - (P_V - P_{IB}) \cdot (P_V - P_{IB})},$$
$$L_{VH} = \sqrt{(P_H - P_V) \cdot (P_H - P_V)}. \tag{17}$$

Using Eqs. (15) and (16), the position vector of S_{OB} in the O-xyz coordinate system can be calculated as

$$P_{OB} = [T_H]^T p_{OB,H} + P_H. \tag{18}$$

For three points on the hub carrier (S_{OB}, H, and S_{KP}), the position vectors p_{OB}, p_H, and p_{KP} in the R_{WC}-$\xi\eta\zeta$ coordinate system and the position vectors P_{OB}, P_H, and P_{KP} in the O-xyz coordinate system have now been found. From these position vectors, the coordinate transformation matrix for rotating from the R_{WC}-$\xi\eta\zeta$ coordinate system to the O-xyz coordinate system is given as

$$[T]^T = [I_{KP} \quad J_{KP} \quad K_{KP}]^T \begin{bmatrix} i_{KP}^T \\ j_{KP}^T \\ k_{KP}^T \end{bmatrix}, \tag{19}$$

where I_{KP}, J_{KP}, and K_{KP} are the ξ_{KP}, η_{KP} and ζ_{KP} axis unit direction vectors as seen in the O-xyz coordinate system and i_{KP}, j_{KP} and k_{KP} are the ξ_{KP}, η_{KP} and ζ_{KP} axis unit direction vectors as seen in the R_{WC}-$\xi\eta\zeta$ coordinate system, for a new moving coordinate system fixed in $\Delta S_{KP} S_{OB} H$, having its origin at S_{KP}, having the direction normal to $\Delta S_{KP} S_{OB} H$ as the ζ_{KP} axis, the $S_{KP} S_{OB}$ direction as the ξ_{KP} axis, and the direction orthogonal to these axes

as the η_{KP} axis. These unit direction vectors can now be calculated using the equations below.

$$I_{KP} = \frac{P_{OB} - P_{KP}}{|P_{OB} - P_{KP}|}, \quad K_{KP} = \frac{I_{KP} \times (P_H - P_{KP})}{|I_{KP} \times (P_H - P_{KP})|}, \quad J_{KP} = K_{KP} \times I_{KP},$$

$$i_{KP} = \frac{p_{OB} - p_{KP}}{|p_{OB} - p_{KP}|}, \quad k_{KP} = \frac{i_{KP} \times (p_H - p_{KP})}{|i_{KP} \times (p_H - p_{KP})|}, \quad j_{KP} = k_{KP} \times i_{KP} \quad (20)$$

The origin of moving coordinate system R_{WC}-$\xi\eta\zeta$ (the center of the front wheel, R_{WC}), and the position vector of the strut bottom end Q in the O-xyz coordinate system are given by:

$$P_{WC} = P_H - [T]^T p_H, \quad (21)$$

$$P_{SB} = [T]^T p_{SB} + P_{WC}. \quad (22)$$

The strut length is given by:

$$q = \sqrt{(P_{SU} - P_{SB}) \cdot (P_{SU} - P_{SB})}. \quad (23)$$

The motions of the suspension-steering mechanism have now all been found for the case in which two inputs (the translational displacement of S_{IB} and the displacement of S_{KP} from the angular displacement of the suspension arm) have been provided for the suspension-steering mechanism. The calculations above are entirely analytical and free from any numerical approximations. While not covered in this article, the velocity, acceleration, angular velocity and angular acceleration of each link or pair can be analytically calculated by time differentiation of all the equations. Analytical application of inverse dynamics analysis could also make it possible to find a mechanism's drive force/drive torque or the forces and moments acting on each pair when the mechanism is performing the desired motion while subject to an external force.

4. Examples of Kinematic Analysis and Motion Performance Evaluation

4. 1 Example of Analysis

This section provides an analysis of a mechanism having the specifications listed in **Table 1**. The values shown are actual measurement values for a mechanism in a given compact FF vehicle. They represent items such as the position vectors in the O-xyz coordinate system fixed to the vehicle body, for kinematic pairs in the suspension-steering mechanism of the right front wheel when the steering amount is zero (during straight-line travel). When the left and right mechanisms are completely symmetrical, the origin O of the O-xyz coordinate system is the midpoint of the centers of the left and right front wheels during straight-line travel, the $+y$ direction is the direction of forward vehicle travel, and the $+x$ direction is the vehicle's right direction. The camber angle and toe

angle of the left and right wheels are considered to be zero during straight-line travel. P_{RP} in the table is the rack bar's center position, P_{SA} is the position of the revolute pair at the base of the suspension arm, K_{SA} is the unit direction vector of the revolute pair in the rotational axis direction, W is the distance between the centers of the left and right wheels, and L is the distance between the front and rear wheel axles during straight-line travel. L_T is the tie rod length and L_S is the suspension arm length, as determined dependently on other values in the table. The rack bar in this example is positioned in front of the front wheel axle.

The mechanism's main constants are the position vectors as seen in the moving coordinate system R_{WC}-$\xi\eta\zeta$ on the hub carrier. They are given by the equations below, from the position vectors given in **Table 1** as seen in the O-xyz coordinate system during straight-line travel.

$$p_{OB} = P_{OB,0} - P_{WC,0}, \quad p_{KP} = P_{KP,0} - P_{WC,0},$$

$$p_{SB} = P_{SB,0} - P_{WC,0}, \quad u_S = \frac{P_{SU} - P_{SB,0}}{|P_{SU} - P_{SB,0}|}. \quad (24)$$

The analysis procedure of **Section 3. 2** was used to analyze the motion of the mechanism having the specifications of **Table 1**. The analysis range is from maximum left-turn steering, to straight-line travel, and to maximum right-turn steering. In other words, the rack bar displacement range is $-s_{max} \leq s \leq s_{max}$ ($s = 0$ during straight-line travel).

Figure 5 shows how the left and right steering angles (θ_L, θ_R) and camber angles (ϕ_L, ϕ_R) vary in relation to rack bar displacement, s, when the suspension arm is fixed as it is during straight-line travel. The steering angle is defined as the angle between the x axis and the xy plane projection of the vector of the ξ axis of the moving coordinate system R_{WC}-$\xi\eta\zeta$ fixed at the center of the front wheel. The camber angle is defined as the angle between the z axis and the yz plane projection of the vector of the ζ axis. The ξ axis of the moving coordinate system fixed at the center of the left front wheel is set so that the vehicle's right direction is positive. The η axis is set so that the vehicle's forward direction is positive. So during straight-line travel, the moving coordinate systems of the left and right front wheels R_{WC}-$\xi\eta\zeta$ have identical postures. The maximum rack bar displacement s_{max} given by the calculation results in a steering angle with an absolute value of $\theta_{max} = 45°$.

The steering angles of **Fig. 5** (a) decrease monotonically relative to rack bar displacement, s. Using $\theta_L = \theta_R = 0°$ for $s = 0$, we can see that θ_L (–s) = –θ_R (s) and θ_R (–s) = –θ_L (s). The camber angles of **Fig. 5** (b) are a characteristic of the MacPherson strut suspension mechanism. As shown, they vary with rack

bar displacement, s, with the wheels tilting in the turning direction. **Figure 5** (c) plots the difference between the right and left steering angles. This left-right difference is generated in accordance with rack bar displacement, s, and illustrates the performance of a feature called the Ackermann-Janteau scheme[1)–6)] that enables lines extending from the axles of the left and right front wheels to intersect.

Table 1 Dimensions of a suspension and steering mechanism to be analyzed

(Unit : mm, except K_{SA})

$P_{WC,0}$	$(730.0,\ 0.0,\ 0.0)^T$	P_{SA}	$(350.0,\ 220.0,\ -68.0)^T$
P_{SU}	$(560.0,\ -57.0,\ 470.0)^T$	K_{SA}	$(0.0324,\ 0.9947,\ -0.0972)^T$
$P_{SB,0}$	$(590.0,\ -5.0,\ 54.0)^T$	W	$1\ 460.0$
$P_{KP,0}$	$(680.0,\ 17.0,\ -86.0)^T$	L	$2\ 500.0$
P_{RP}	$(0.0,\ 77.0,\ 48.0)^T$	L_T	414.38
$P_{IB,0}$	$(280.0,\ 77.0,\ 48.0)^T$	L_S	387.86
$P_{OB,0}$	$(690.0,\ 120.0,\ 6.0)^T$		
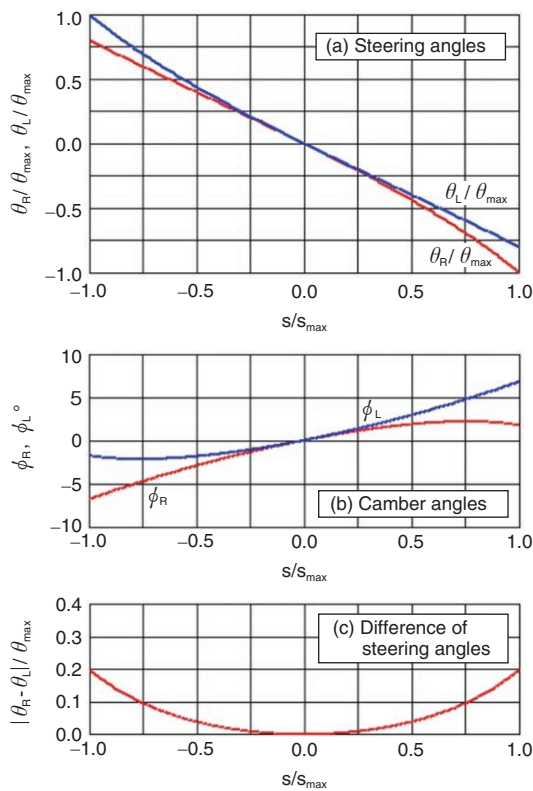
Fig. 5 The analyzed steering and camber angles

Figure 6 plots the circles in the center of the width direction of the mechanism and wheels, showing plots of four postures (s/s_{max} = –1, –0.5, 0, 0.5, 1). The white circles in the graph are the spherical pairs at the tie rod ends (S_{IB} and S_{OB}), the red circles are the wheel centers (R_{WC}), and the blue circles are the kingpins (S_{KP}). As shown, the camber angle increases and the wheel center position fluctuates as the vehicle turns.

Figure 7 shows the effect of the suspension arm angular displacement ψ on the right wheel steering angle and camber angle when $s = 0$ and $s = s_{max}$. Δq in the graph is the strut length variation. The graph shows that the camber angle increases as the strut extends, and then decreases from strut contraction due to centrifugal force once the turn outer ring has been reached. The graph also shows that the effect on the steering angle is small during straight-line travel.
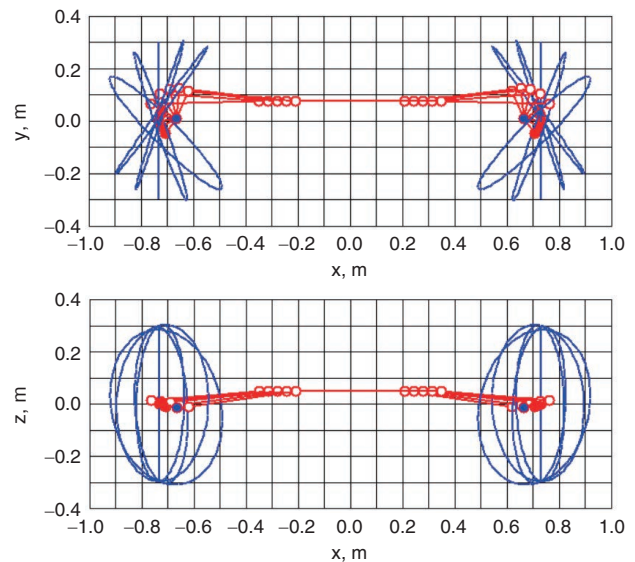
Fig. 6 Skeleton diagram of the mechanism while steering
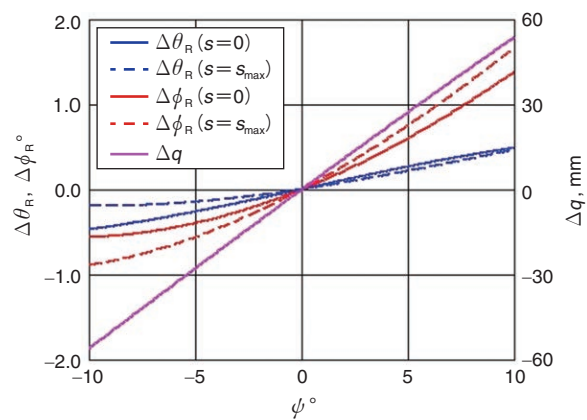
Fig. 7 Effect of suspension input

4. 2 Motion Performance Evaluation

This section uses the analysis results to evaluate the suspension and steering mechanism's motion performance.

4. 2. 1 Turning Center Fluctuation

Turning center fluctuation is the first item for evaluation. **Figure 8** shows wheel motion during an ideal turn, which has been covered by several different literatures. Assuming a camber angle of zero and looking at the xy plane, the vehicle's turning center is defined as the point C where lines extending from the axles of the steered front wheels intersect a line extending from the rear wheel axle. Being able to steer the two front wheels in this way is held to prevent skidding. But the one degree of freedom of the steering mechanism makes it impossible to perfectly execute this type of ideal steering, resulting in turning center position fluctuation. In other words, lines extending from the axles of the two front wheels intersect a line extending from the rear wheel axle at C_L and C_R as shown in **Fig. 9**. The midpoint of these two intersection points is defined as the virtual turning center C, and the distance between the coordinate system's origin O (the midpoint between the two front wheel centers) and C is defined as the turning radius R. As shown in the equation below, let the turning center fluctuation assessment be defined as the sum of the absolute values of the angles ($\Delta\theta_L$ and $\Delta\theta_R$) formed by the central axis of each front wheel and the line segment OC.

$$\kappa = |\Delta\theta_L| + |\Delta\theta_R| \tag{25}$$

Before evaluating the mechanism, the ideal steering angle first needs to be considered. Given a right front wheel steering angle $\theta_R(s)$ within the rack bar displacement range $0 \le s \le s_{max}$ (right turn), the left front wheel steering angle $\theta_L(s)$ can be determined. The x coordinate of turning center C in **Fig. 8** is given geometrically by:

$$x_{TC} = \frac{W}{2} - L\cot\theta_R(s). \tag{26}$$

When the straight line passing through the axle of the left front wheel passes through point C, the left front wheel steering angle $\theta_L(s)$ is given by:

$$\theta_L(s) = -\tan^{-1}\frac{L}{W - L\cot\theta_R(s)} \tag{27}$$

For a left turn, $\theta_L(-s) = -\theta_R(s)$ and $\theta_R(-s) = -\theta_L(s)$ can be used as described previously. So $\theta_R(s)$ should be set in a form enabling smooth steering ranging from a left turn, to straight-line travel, to a right turn. The conditions for $\theta_R(s)$ are set as follows:

(1) $\theta_R(0) = 0$
(2) $\theta_R(s_{max}) = -\theta_{max}$
(3) The first and second derivatives of $\theta_R(s)$ are continuous during left and right turns.
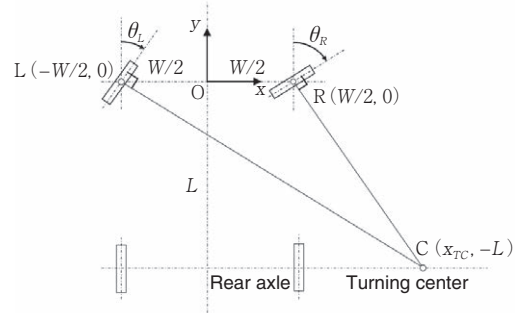
Fig. 8 Ideal steering motion
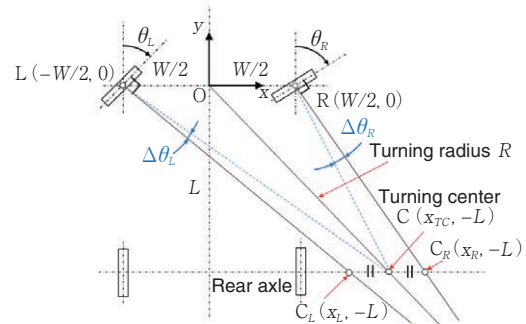
Fig. 9 Actual steering motion

If $\theta_R(s)$ were given as a linear function of s for example, Condition (3) would clearly not be satisfied. So the function will be given in the following form:

$$\theta_R(s) = C_0 + C_1 s + C_2 e^{\lambda s} \tag{28}$$

where C_0, C_1 and C_2 are unknown coefficients and λ is a constant. The exponential function term has been added to provide variation in the rate of change with respect to s. The constant term C_0 has been added on the other end as an adjustment used to satisfy the condition $\theta_R(0) = 0$.

Conditions (1) and (2) above yield the equations below.

$$C_0 = \frac{\theta_{max} + C_1 s_{max}}{e^{\lambda s_{max}} - 1}, \quad C_2 = -C_0 \tag{29}$$

So C_0, C_1 and C_2 are given by linear functions of C_1. Condition (3) now yields the equation below (details omitted).

$$\frac{d}{ds}\theta_L(0) = \frac{d}{ds}\theta_R(0) \tag{30}$$

So first derivative continuity has been established. Now from the condition of second derivative continuity, using

$$\frac{d^2}{ds^2}\theta_R(0) = \frac{d^2}{ds^2}\theta_L(0) \tag{31}$$

yields the equation below by solving for C_1 (details again omitted).

$$C_1 = \frac{-b + \sqrt{b^2 - 4ac}}{2a}, \tag{32}$$

where,

$$a = W(1+\lambda d)^2, \quad b = \lambda(2W\lambda de + 2We + L\lambda d),$$

$$c = \lambda^2 e(We+L), \quad d = \frac{-s_{\max}}{e^{\lambda s_{\max}}-1}, \quad e = \frac{-\theta_{\max}}{e^{\lambda s_{\max}}-1} \tag{33}$$

So a steering angle function that satisfies Conditions (1) to (3) for a given λ has been found.

Figure 10 shows the calculation results for the ideal steering angle function when $\lambda = 5.0$. As shown, the derivative is continuous. The turning center fluctuation assessment here is always $\kappa = 0$. Comparing these results to **Fig. 5** reveals a large difference between the left and right steering angles.

Now we'll evaluate steering performance for the example analysis of **Fig. 5**. **Figure 11** (a) plots the turning radius. **Figure 11** (b) plots $\Delta\theta$—the difference between the $\theta_L(s)$ values of **Fig. 5** and the $\theta_L(s)$ values calculated from Eq. (27) using the $\theta_R(s)$ results of the example analysis. **Figure 11** (c) shows turning center fluctuation assessment κ (Eq. (25)). **Figures 11** (b) and **11** (c) show that turning center fluctuation increases as the absolute value of the steering angle increases.

4. 2. 2 Motion Transmissibility Evaluation

This section evaluates whether steering can be executed without any statical problems caused by either turning center fluctuation or rack bar linear displacement, s. When
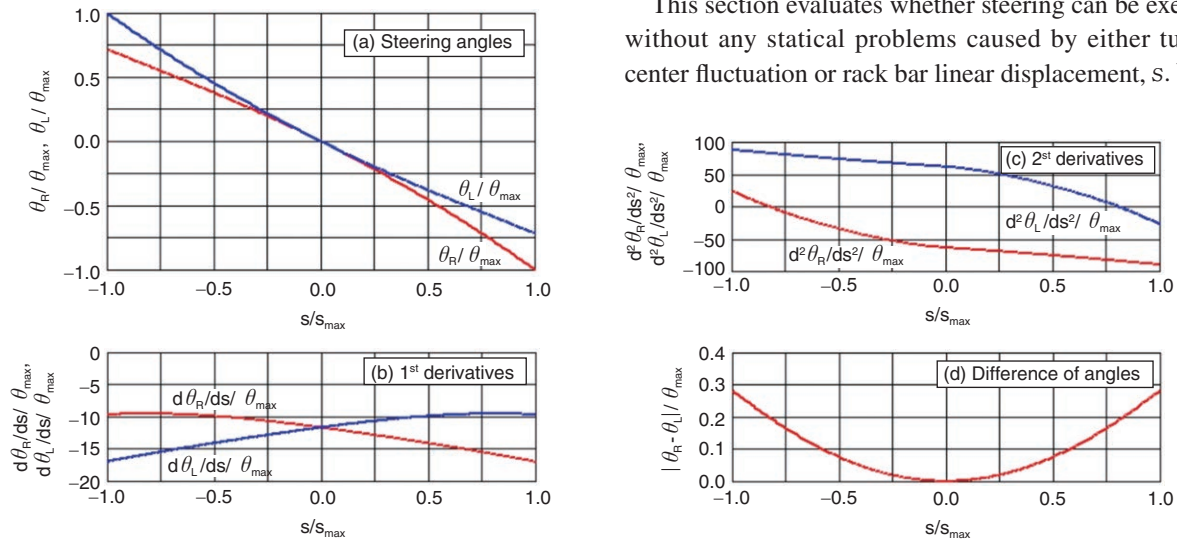
Fig. 10 Ideal steering angle function
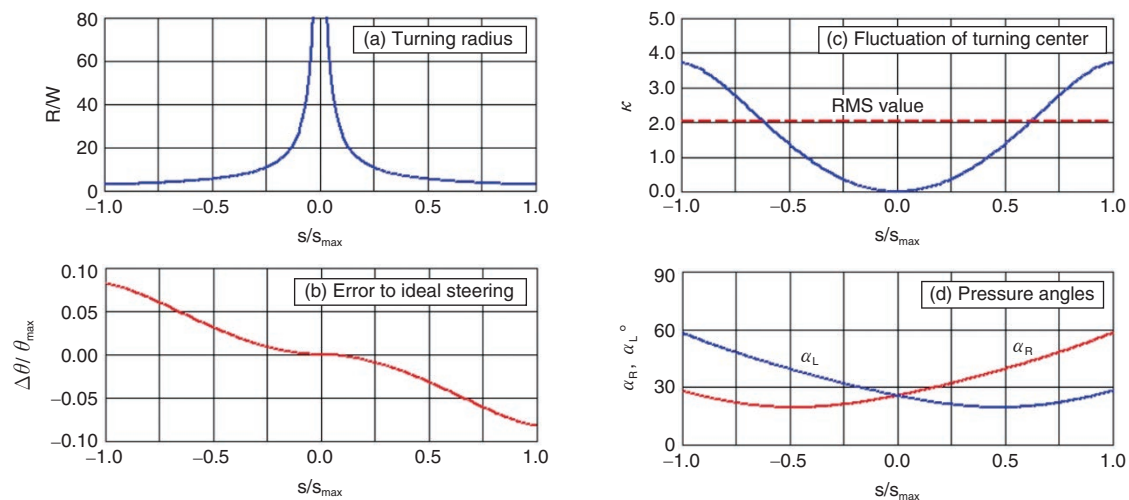
Fig. 11 Motion performance evaluation of the analyzed mechanism

suspension mechanism strut displacement is ignored and the kingpin axis is considered a revolute pair at point H, the steering mechanism of **Fig. 3** can be considered a spatial slider crank composed of a rack bar, tie rod and knuckle arm. So the pressure angle α between the tie rod and knuckle arm can be evaluated. From **Fig. 3**, α can be calculated as

$$\alpha = \left| \cos^{-1}\left[\left(U_K \times \frac{P_{OB} - P_H}{|P_{OB} - P_H|} \right) \cdot \frac{P_{OB} - P_{IB}}{|P_{OB} - P_{IB}|} \right] \right|. \tag{34}$$

Figure 11 (d) plots the change in pressure angles between the left and right tie rods and knuckle arms of the example analysis. As shown, the pressure angles increase as the absolute value of the steering angle increases.

5. Optimum Design

An attempt was made to derive the optimum design using the mechanism performance indexes covered in **Section 4**. The design covers the steering mechanism only, leaving the MacPherson strut suspension mechanism specifications unchanged. Specifically, the mechanism's performance was improved by changing the rack bar position, rack bar length, tie rod length, and the position of the spherical pair connecting the tie rod and knuckle arm on the hub carrier. But to satisfy the straight-line travel condition applicable when rack bar displacement $s = 0$, the six component variables of the kinematic pair position vectors $P_{IB, 0}$ and $P_{OB, 0}$ for the straight-line travel state of **Table 1** are handled as design variables.

The ideal steering angle function of Eqs. (27) and (28) explained in **Section 4** could be set as the objective function for optimization, and the generated steering angle functions could be optimized to match it. But that approach would be difficult and not enable motion transmissibility to be evaluated at the same time.

Instead, κ_{RMS} is used as the turning center fluctuation objective function for optimization and $\alpha_{\max}$ as the motion transmission characteristic objective function for optimization. κ_{RMS} is the RMS value of evaluation index κ within the rack bar's permissible movement range, and $\alpha_{\max}$ is the maximum value of pressure angle α between the tie rod and knuckle arm. Since lower values are more desirable for both of these variables, optimization is carried out to minimize the objective function.

The first step is to estimate how the objective functions change in response to minute adjustments to these design variables. **Figure 12** shows how objective functions κ_{RMS} and $\alpha_{\max}$ are affected by minute changes made to the **Table 1** value of each design variable independently (the p of Δp is the applicable design variable). While naturally these plots only show results in the neighborhood of the **Table 1** values, they show that the x

position of the spherical pair S_{IB} ($x_{IB, 0}$) and the y position of the spherical pair S_{OB} ($y_{OB, 0}$) have high sensitivity and increase or decrease in inverse correlation to the two objective functions κ_{RMS} and $\alpha_{\max}$.
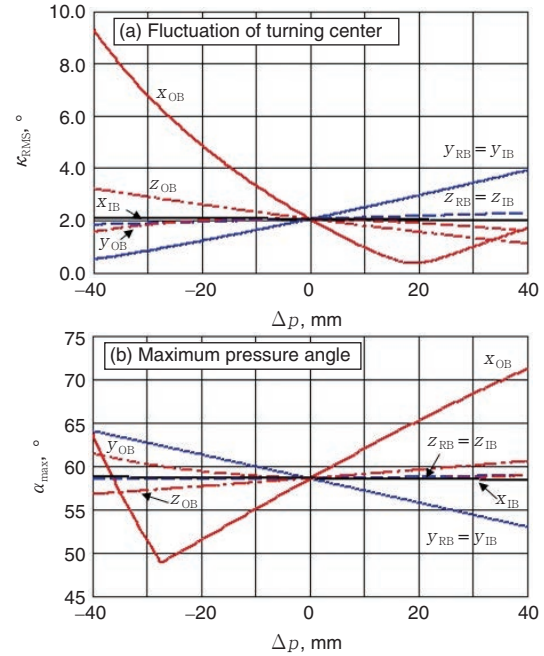
Fig. 12 Variation of performance evaluation criteria due to design variables

So to cover both of the objective functions, the six design variables are optimized using the equation below (the linear sum of both functions) as the objective function.

$$\Phi\left(x_{IB, 0}, y_{IB, 0}, z_{IB, 0}, x_{OB, 0}, y_{OB, 0}, z_{OB, 0} \right)$$
$$= w_1 \kappa_{RMS} + w_2 \alpha_{\max} \tag{35}$$

The downhill simplex method[14] is used as the optimization method, with suitable side constraints imposed on the design variables to account for the space occupied by the mechanism. The $s_{\max}$ value is also corrected each time to keep the maximum steering angle at $\theta_{\max} = 45°$, since changing the mechanism specifications could result in different maximum steering angle $\theta_{\max}$ values for the same rack bar maximum displacement $s_{\max}$ value.

Figure 13 shows the optimization result for (w_1, w_2) = (1.0, 0.0), which covers only turning center fluctuation. **Figure 13** (a) shows the turning center fluctuation index κ, **Fig. 13** (b) shows the pressure angles α, and **Figs. 13** (c) and (d) are skeleton diagrams. As shown in the graph, there is significant reduction in index κ. But the maximum pressure angle is slightly larger than the initial value, and the motion transmission characteristic deteriorates despite an improvement in turning performance.

Figure 14 shows the optimization result for $(w_1, w_2) =$ (1.0, 12.0). The graphs show that the resulting mechanism managed to improve on the initial values for both the turning center fluctuation index κ and the pressure angles α, indicating that the multi-objective optimization was successful. The resulting mechanism has a longer rack bar but a shorter tie rod. A longer rack bar might not necessarily be beneficial as problems from its elastic deformation could be foreseen. Although handled by the side constraints imposed on the design variables, spherical pair S_{OB} is positioned fairly close to the wheel center. So the space occupied by the mechanism that was not accounted for by this article should possibly also be added to the objective functions for optimization.
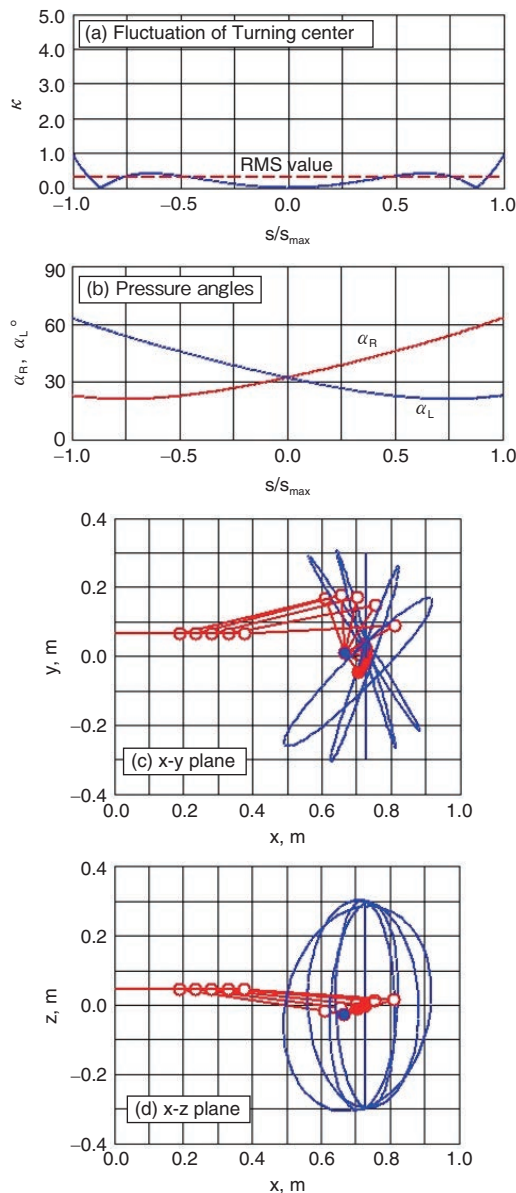
Fig. 13 Optimization result 1
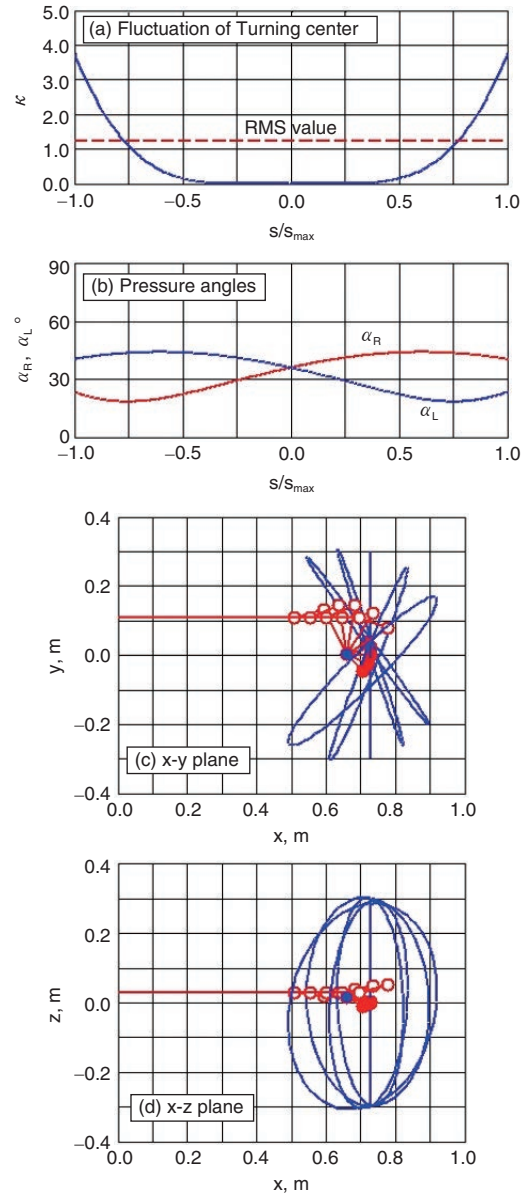
Fig. 14 Optimization result 2

6. Conclusion

To gain an understanding of the workings and motions of vehicle suspension and steering mechanisms, this article has presented the example of a MacPherson strut suspension mechanism and a steering mechanism driving a hub carrier using a rack bar and tie rod. The kinematic analysis of these mechanisms as a spatial link mechanism with 2 degrees-of-freedom was explained. By using the analysis, the motion performance evaluation was carried out and the optimum design with the evaluated quantities as objective function was tried.

While the kinematic analysis method is not new, a simple explanation of it has been provided in the form of vector analysis based on the essence of the spatial geometry determining the mechanism motion. This

analysis procedure has not used any numerical analysis or other approximation analysis. So all the motion displacements derived in this article could be analytically time-differentiated to enable velocity or acceleration analysis. The acceleration could then be used with inverse dynamics analysis to determine all the dynamic forces and moments acting on each link or pair in a mechanism. The author hopes that these analyses are applied to future design.

The optimum design example presented in this article yielded a mechanism with superior performance relative to the initial mechanism. However, the occupied space of the mechanism is taken into account only by giving side constraints for the design variables, the actual occupied space is therefore expected to be added to the objective functions. But this addition may diminish the best performance currently obtained because the original initial mechanism was designed from actual vehicle measurement values and must already be close to the optimum solution.

The author hopes this article will be able to provide some help to readers working on mechanical analysis and design.

References

1) Teruo ITSUKI: Automotive Engineering (3rd Edition), Ohmsha (2020) (in Japanese).

2) Motoo AOYAMA: Mechanisms in Automobiles, Natsumesha (2021) (in Japanese).

3) Osamu FURUKAWA Ed.: Perfect Encyclopedia on Automobile, Natsumesha (2021) (in Japanese).

4) Yoji IIJIMA: Basic Knowledge of Automobile Suspension, Nikkan Kogyo Shinbun (2018) (in Japanese).

5) Yasuo TAKAHASHI: Basic Knowledge of Automobile Mechanisms (Continued) -Step up Edition-, Nikkan Kogyo Shinbun (2022) (in Japanese).

6) Masato ABE: Automotive Vehicle Dynamics - Theory and application – (2nd Edition), Publishing Office, Tokyo Denki University (2012) (in Japanese).

7) CRONIN, D.L.: MacPherson Strut Kinematics, Mechanism and Machine Theory, 16-6 (1981) pp. 631-644.

8) FELZIEN, M.L., CRONIN, D.L.: Steering Error Optimization of the MacPherson Strut Automotive Front Suspension, Mechanism and Machine Theory, 20-1 (1985) pp. 17-26.

9) KANG, H.Y., SUH, C.H.: Synthesis and Analysis of Spherical-Cylindrical (SC) Link in the McPherson Strut Suspension Mechanism, Trans. ASME, Journal of Mechanical Design, Vol. 116 (1994) pp. 599-606.

10) DANIEL A. MANTARAS, PABLO LUQUE, CARLOS VERA: Development and validation of a three-dimensional kinematic model for the McPherson steering and suspension mechanisms, Mechanism and Machine Theory, 39 (2004) pp. 603-619.

11) Jyun NANGO, Mitsuhito NAGAO and Hiroshi KONNO, Kinematic Analysis of MacPherson Strut Mechanism, Transactions of JSME (Ser. C), 74-747 (2008) pp. 2816-2825.

12) K. VIKRANTH REDDY, MADHU KODATI, KISHEN CHATRA, SANDIPAN BANDYOPADHYAY: A comprehensive kinematic analysis of the double wishbone and MacPherson strut suspension systems, Mechanism and Machine Theory, 105 (2016) pp. 441-470.

13) Takahiro ARUGA and Nobuyuki IWATSUKI: Kinematic Analysis of Spatial Closed-loop Link Mechanisms Based on Spatial 3-link Prime Structures, Proc. of the 4th International Jc-IFToMM Symposium, (2021) pp. 1-8.

14) NELDER, J. A, MEAD, R.: A simplex method for function minimization, The Computer Journal, Vol. 7, Issue 4, (1965) pp. 308-313.